Closed-orbit theory for molecules in fields

A. Matzkin, P. A. Dando, and T. S. Monteiro

Department of Physics and Astronomy, University College London, Gower Street, London WC1E 6BT, United Kingdom
(Received 7 February 2002; published 24 July 2002)

Closed-orbit theory was initially developed as a qualitative and quantitative tool to interpret the dynamics of excited hydrogen in static external fields: the modulations in the photoabsorption spectrum were explained in terms of classical orbits closed at the nucleus. We consider the closed-orbit theory formalism appropriate for molecules in fields. The theoretical extensions are described, and semiclassical calculations based on this formalism are undertaken and compared to quantum *R*-matrix calculations for model molecules in a static magnetic field. We find that the spectral modulations can be analyzed simply in terms of the scattering of the excited electron on the molecular core. In addition to elastic scattering, modulations produced by inelastic scattering are essential to account for the photoabsorption spectrum. Through this process, an electron along a closed orbit in the classically chaotic regime exchanges energy with the core and comes out along an orbit in the near integrable regime. The relative importance of elastic and inelastic scattering depends on the molecular quantum defects.

I. INTRODUCTION

The hydrogen atom in a magnetic field is a well-known [1] paradigm of "quantum chaos"—the study of quantum systems possessing a classically chaotic counterpart. Indeed, a highly excited Rydberg electron in a static magnetic field senses both the spherical Coulomb and the cylindrical magnetic fields; classically, the system is nonseparable, and the trajectories are chaotic. Quantum mechanically, the photoabsorption spectrum displays complex structures. Ever since the quasi-Landau oscillations in the photoabsorption spectrum of barium were associated with the classical motion of the electron in the plane perpendicular to the field axis [2,3], the large-scale structures of such spectra have been associated with classical orbits. This correspondence was highlighted further by taking advantage of scaling properties possessed by those systems. The external fields then play the role of an effective Planck constant, and the quantum system can be studied, theoretically or experimentally, at some fixed dynamical classical regime while effectively changing the Planck constant.

A major advance was achieved with the advent of closed-orbit theory, first introduced for the hydrogen atom by Bogomolnyi [4] and by Du and Delos [5], and developed to a large extent by Mao *et al.* [6], Gao and Delos [7], and Main *et al.* [8]. Closed-orbit theory consists of a fully quantitative approach in which the large-scale structures of the photoabsorption spectra are explained in terms of classical trajectories closed at the nucleus, i.e., those that leave from and return to the core. Each orbit produces on its return an oscillation in the photoabsorption cross section; the Fourier transform of the spectrum, known as the *recurrence spectrum*, therefore exhibits sharp peaks at the period (or scaled action, if the scaling properties are used) of the orbits. Experimental and theoretical recurrence spectra for hydrogen in a magnetic field were found to be in very good agreement [8]. The same closed-orbit formalism can also be applied to study the absorption spectrum in a strong electric field: only the properties of the classical trajectories (which are not chaotic in this case) need of course to be modified.

Closed-orbit theory was also extended to treat the case of nonhydrogenic Rydberg atoms. In addition to the strongly back-focused Coulomb scattered waves, which lead to repetitions of the closed orbits in the hydrogenic case, the phase shifts induced by the core on the electron's wave function—traditionally known as quantum defects—give rise to core-scattered waves. Gao and Delos [7] incorporated the quantum defects in the closed-orbit formalism but concluded that, for the system under consideration, the effect of the core-scattered waves was insignificant and could be omitted from the final formulas. However, the first fully quantum-mechanical calculations for nonhydrogenic atoms in a magnetic field at fixed scaled energies [9] showed strong resonance structures in the recurrence spectra, which seemingly could not be explained by closed orbits of the hydrogenic problem, together with a reduction in the recurrence strength of the contributions from the long-period orbits. These observations were confirmed subsequently by experimental measurements of diamagnetic helium atoms and the additional peaks identified as being due to *combinations* of hydrogenic closed orbits that arise from scattering with the core [10]. Similar structures were also observed in the experimental spectra of lithium atoms in a static electric field [11].

In an attempt to provide a semiclassical description of these additional peaks, two differing approaches were proposed. One approach [12], treated the core-Rydberg electron interactions by employing a model potential which led to the creation of new orbits. This method involved the calculation of several thousand orbits (compared to a couple of dozen for the hydrogen atom at the same scaled energy) and gave only a global qualitative agreement.

An alternative approach [13], which allowed for the breakdown of classical path methods at the core, was more successful. Here, the core-scattered modulations were described as resulting from successive diffractive encounters of the Rydberg electron with the core: the wave function follows the well-known *hydrogenic* classical orbits in the region where the Coulomb and the external fields compete (the "outer region"), but near the core, where the external fields

are negligible (the "inner region"), the wave function is described quantum mechanically. Good quantitative agreement between quantum calculations and closed-orbit theory for an atom with a quantum defect $\mu_{l=1} = 0.5$ was obtained both for the diamagnetic and Stark photoabsorption spectra.

In the present paper, we follow the latter approach to extend closed-orbit theory to the more general case of multichannel core scattering. Indeed, up to now, only single-channel scattering has been assumed. However, a typical Rydberg atom does experience multichannel scattering, in which both the quantum state of the core and of the Rydberg electron may change during the collision. This is also the case for even the simplest molecules, which present multiple Rydberg series converging to different ionization thresholds. General Rydberg atoms and molecules in the field-free case are described by a formalism known as multichannel quantum-defect theory (MQDT) [14,15]. Here, our multichannel extension will be more specifically focused to treat photoabsorption for molecules in a strong magnetic field. The same method may be used for atoms (by changing the quantum numbers and the frame transformation elements) or for other choices of external fields (by changing the parameters of the classical trajectories). The heart of our approach relies on connecting the Green's functions in the inner and outer regions. In the inner region, the Green's function is extracted from the MQDT wave functions by following the method described in [16]; propagation in the outer region is achieved as in the usual form of closed-orbit theory by following the formalism due to Maslov and Fedoriuk [17]. Recently, an alternative approach merging MQDT and closed-orbit theory with the aim of treating multichannel core scattering was presented [18]; rather than directly matching Green's functions, this approach is based on a semiclassical approximation to the long-range scattering matrix, representing the phase accumulated in the outer region and obtained from the semiclassical Green's function. Only model calculations were presented in [18].

Rydberg molecules in a strong magnetic field have received little attention, especially if compared to the countless experimental and theoretical studies performed on atoms. Indeed, even the linear Zeeman effect, which is trivial for atoms, induces mixing between different rotational core states. This was first seen in calculations for the photoabsorption cross section from the ground state of H_2 [19]. It was also experimentally observed in NO, and a detailed theoretical account using MQDT of the uncoupling of the electron from the core for moderately low-Rydberg states was given [20]. However, for higher-Rydberg states, the diamagnetic interaction dominates, which ruins any attempt to explain the dynamics on a MQDT basis. Although R-matrix calculations have been undertaken successfully for H_2 [21], a dynamical interpretation of the photoabsorption spectra seems only possible by resorting to semiclassical analysis. This has been achieved only recently and the results were reported in [22]: the spectral modulations were interpreted in terms of elastic and inelastic diffractive scattering of the Rydberg electron on the molecular core.

The present paper is organized as follows. In Sec. II, we give a brief summary of *atomic* closed-orbit theory, together with the basic equations. Section III presents multichannel molecular closed-orbit theory. We first give an overview of the physics of such systems, and then go into a detailed presentation of the formalism. Section IV describes the method employed to perform quantum calculations. Our results are presented in Sec. V: we compare quantum and semiclassical calculations for various "model" molecules having different quantum defects. It will be seen that the appearance of the recurrence spectra are indeed governed by the core-scattering process. The inclusion of some higher-order effects (in $\hbar$) is also discussed. Finally, in Sec. VI, we present our conclusions. Atomic units are used throughout, with the $\hbar$ factors reestablished where appropriate.

II. CLOSED-ORBIT THEORY

In atomic closed-orbit theory, two different regions of space are identified: a region near the core ($r < r_0$; $r_0 \sim 50$ Bohr radii) where the external field can be neglected but a quantum description is required, and an outer region ($r > r_0$) where a semiclassical description is feasible. When the atom absorbs a photon, the excited electron leaves the core region in a near zero-energy outgoing Coulomb wave at an initial angle θ_i, to the field direction. For $r > r_0$, the wave propagates semiclassically, following classical trajectories. Eventually, these trajectories are turned back by the combined action of the Coulomb potential and the external field. Some of the trajectories return to the vicinity of the core region at an angle of incidence θ_f, to the field direction. Here again a quantum description is needed and a scattering wave function can be constructed. The outgoing part of the scattered wave is comprised of two components: a *Coulomb* scattered wave and, for nonhydrogenic atoms, *core-scattered* waves. The Coulomb scattered waves are strongly back focused and result in repeated traversals of the trajectory. The core-scattered waves redistribute amplitude into other closed orbits.

The result is a formula for the average oscillator-strength distribution f, that consists of a slowly varying background term f_{back}, together with an oscillatory part f_1, involving a sum of contributions over all closed orbits k, of the system,

$$f_1(E) = -\frac{2(E-E_0)}{\pi} \text{Im} \sum_k \mathcal{N}_k \langle D\Psi_0 | \Psi_{ret} \rangle, \qquad (1)$$

which arises from the interference between the returning wave scattering at the core, and the original outgoing wave. Here, $(E-E_0)$ is the energy of the electron with respect to the zero-field ionization limit of the atom E_0, the wave function of the initial state from which the laser excitation occurs is denoted by Ψ_0, D is the component of the dipole operator relevant for the polarization of the exciting laser, and Ψ_{ret} is the wave function of the returning wave scattered at the core.

The coefficients $\mathcal{N}_k$, are calculated by matching the semiclassical wave returning to the core with the incoming part of the scattered wave function $\Psi_{inc}(r_0, \theta_{fk})$ at the boundary $r = r_0$. The resulting matching equation is

$$\Phi_0(r_0,\theta_{ik})\mathcal{A}_k e^{i(S_k+\phi_k)}=\mathcal{N}_k\Psi_{\text{inc}}(r_0,\theta_{fk}), \qquad (2)$$

where $\Phi_0(r_0,\theta_{ik})$ is the initial outgoing wave function at $r=r_0$ needed to construct the semiclassical wave function. S_k is the classical action of trajectory k, and ϕ_k is an additional phase term. The effective amplitude $\mathcal{A}_k$ is related to the classical amplitude which, in turn, depends upon the stability and topology of the orbit.

A. Hydrogen

In the case of hydrogen, the initial outgoing Coulomb wave $\psi_{\text{out}}(r_0,\theta)$, at the boundary between the semiclassical and quantum region is used as a starting condition for constructing the semiclassical wave

$$\Phi_0(r_0,\theta_{ik})=\psi_{\text{out}}(r_0,\theta_{ik}). \qquad (3)$$

The calculated $\mathcal{N}_k$ are then proportional to $\mathcal{A}_k e^{iS_k}$. The kth closed orbit thus leads to an oscillation with frequency S_k and amplitude $\mathcal{A}_k$ in the absorption spectrum. Coulomb scattering is focused strongly backward and may result in repeated traversals of the orbit; these are connected to harmonics in the oscillator strength distribution.

The Hamiltonian of the hydrogen atom in external fields can be scaled exactly. The scaling results in removing the separate dependence of the Hamiltonian on the electron energy and the field intensity by a dependence on a sole parameter, the scaled energy ϵ. This is shown in Appendix A in the case of an external magnetic field.

B. Nonhydrogenic atoms

In an extension of closed-orbit theory, Gao and Delos [7] incorporated the effects of the ionic core in the closed-orbit sum. As well as considering the quantum defects that describe the nonhydrogenic nature of the core, Gao and Delos also included the effects of the nonhydrogenic radial dipole integrals and spin-orbit coupling in the initial state; these quantities all affect the angular distribution of the outgoing waves. However, the effect of the nonhydrogenic core-scattered waves was found to be negligible for the system considered and hence omitted in the final calculation.

In order to reproduce successfully resonance structures observed in the Fourier transformed spectra (the "recurrence spectra") of nonhydrogenic atoms in static magnetic [10] and electric [11] fields, Dando *et al.* [13] included the core-scattered waves consistently within the closed-orbit formalism. For a nonhydrogenic atom, the scattered quantum wave function consists not only of an incoming part returning to the core and a Coulomb part scattered back in the direction of the incoming trajectory but also of an additional outgoing, core-scattered wave

$$\Psi_{\text{ret}}(r,\theta)=\Psi_{\text{inc}}(r,\theta)+\Psi_{\text{Coulomb}}(r,\theta)+\Psi_{\text{core}}(r,\theta). \qquad (4)$$

The effect of the core-scattered waves is to redistribute amplitude into all other closed orbits.

To incorporate the effect of the core-scattered waves in the closed-orbit sum, the extra outgoing waves are added to the starting condition for constructing the semiclassical wave function [13]

$$\Phi_0(r_0,\theta_{ik})=\psi_{\text{out}}(r_0,\theta_{ik})+\sum_q \mathcal{N}_q\Psi_{\text{core}}^q(r_0,\theta_{ik}). \qquad (5)$$

Substituting this expression for Φ_0 into Eq. (2) gives the following equation for the coefficients, $\mathcal{N}_k$:

$$\mathcal{N}_k\Psi_{\text{inc}}(r_0,\theta_{fk})=\left[\psi_{\text{out}}(r_0,\theta_{ik})+\sum_{q,p}\mathcal{N}_q\Psi_{\text{core}}^q(r_0,\theta_{ik})\right]\sum_n \mathcal{A}_k^n e^{i(S_k^n+\phi_k)}. \qquad (6)$$

The first term on the right-hand side of Eq. (6) accounts for the oscillation due to the hydrogenic orbit k, the second term accounts for all combination orbits for which the electron is finally core scattered from an orbit q into the orbit k. The harmonics of k and q are labeled by n and p, respectively.

The resulting matching equation [Eq. (6)] now has $\mathcal{N}$ values on both sides and this is most conveniently solved by an iterative procedure. We begin by setting $\mathcal{N}_q$ on the right-hand side of Eq. (5) to zero and obtain a first approximation to $\mathcal{N}_k$; this is equivalent to the hydrogenic closed-orbit result. In each successive step extra terms of the form, $\mathcal{A}_q\cdots\mathcal{A}_k e^{i(S_q+\cdots+S_k)}$, are added to the previous result. The resulting recurrence spectrum thus shows two effects not seen in the hydrogenic case. First, the core casts a "shadow" in the backward direction changing the recurrence strength of subsequent returns to the core of each trajectory. Second, there are "combination recurrences" due to the electron traveling along one closed orbit and then being scattered by the ionic core on to another closed orbit. In successive steps of the iterative process combinations of more and more orbits are included.

III. CLOSED-ORBIT THEORY EXTENDED TO MOLECULES IN FIELDS

We give in this section the developments needed to understand molecules in fields within the framework of closed-orbit theory. From a formal point of view, the main difference with the results reviewed in Sec. II concerns the treatment of the core region. Indeed, the dynamics of a Rydberg electron along closed orbits in the outer region is identical here to the atomic case, but the core scattering which governs the way the orbits are combined is intrinsically a multichannel process, which gives rise to effects, such as inelastic scattering. Hence, the inner zone treatment will be based on molecular multichannel quantum-defect theory (MQDT), which describes Rydberg molecules in field-free situations. In the developments that follow below, we shall make some simplifying assumptions; in particular, we will disregard electronic interactions and vibrational couplings, which can be very important in many molecules or specific

symmetries thereof, as well as spin. We expect our model to be adequate for a simple diatomic molecule such as H_2 when photoabsorption takes place from the ground state to the $l = 1$ ungerade complex. We detail below the extension of closed-orbit theory for such a model. We have tried to follow the standard notation of quantum-defect theory (see Appendix B) to describe the phenomena in the inner zone. However, to allow for a direct comparison with earlier results in closed-orbit theory, we have chosen to keep to the conventions (e.g., for normalization) usually employed in closed-orbit related works, originally introduced in [5].

A. General picture

1. Dynamical couplings

Generally speaking, MQDT is based on the separation of the long-range Coulomb field from the short-range effects induced by the core (see Appendix B). These short-range effects produce phase shifts in the wave function of the outer electron. Furthermore, the dynamics of a molecular Rydberg electron in the field-free situation falls in one of two situations. Near the core, the electron is strongly coupled to the molecular axis and is best described in the molecular (Born-Oppenheimer) basis, with good quantum numbers $|\alpha\rangle \equiv |\Lambda_\alpha J_\alpha l_\alpha\rangle$; Λ is the projection of the electronic angular momentum on the molecular axis, l is the orbital momentum of the outer electron, quantized along this axis, and J gives the total angular momentum. Far from the core, $|i\rangle \equiv |N_i l_i\rangle^{JM}$ is an appropriate basis in the field-free situation (J is conserved, M is its projection on a space-fixed axis, and N is the angular momentum of the freely rotating core). But in the presence of a magnetic field, only the axial symmetry remains, i.e., J is not conserved but its projection M on the field axis is; then $|j\rangle \equiv |N_j l_j m_j\rangle^M$ is an appropriate basis (l is now quantized in the laboratory frame along the axis of the magnetic field with magnetic quantum number m_j, and $M = M_{N_j} + m_j$). Hence, far from the core the electron precesses around the field axis. The uncoupling of the electron dynamics from the core may thus be seen as proceeding in two steps, from the $|\alpha\rangle$ basis to $|i\rangle$ then from $|i\rangle$ to $|j\rangle$ [20], or alternatively by obtaining a single orthogonal transformation from the $|\alpha\rangle$ basis to the $|j\rangle$ one, as originally proposed by Monteiro and Taylor [19] where the transformation elements $\langle j|\alpha\rangle$ are given explicitly. In what follows, we shall omit the explicit dependence of the uncoupled basis and transformation elements on M (an independent calculation must be performed for each value of M).

2. Physical picture

As in the atomic case, we divide space into an *inner* region around the core, where the magnetic field is negligible compared to the Coulomb interaction, and an *outer* region where the quadratic Zeeman and Coulomb interactions compete. The global picture can be staged in eight different steps (see Fig. 1): (1) The molecule in its ground state, compactly localized around the core, is excited by a laser; (2) the excited electron uncouples from the core. The outgoing waves are propagated quantum mechanically until (3) the electron
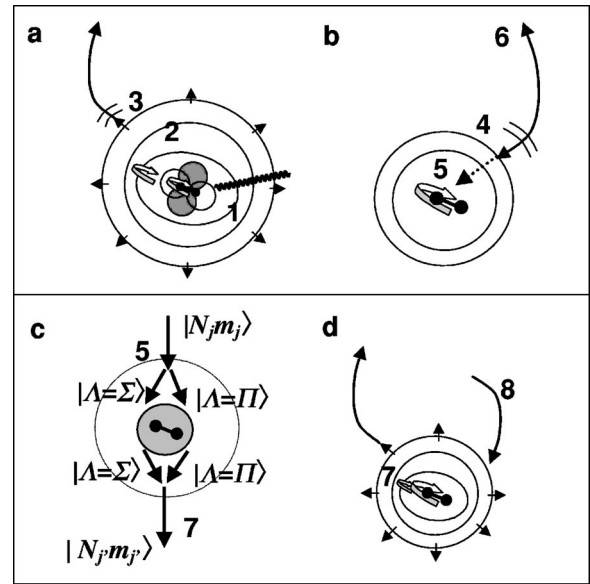

FIG. 1. Simplified picture of the photoabsorption process giving rise to recurrence spectra. Each numbered step is described in the text. Panel *a* shows the photoexcitation process (1); the wave function of the excited electron propagates quantum mechanically in the inner zone (2); and semiclassically in the outer zone (3); the radius of the outer circle is at about 50 a.u., and the waves travel outward a few thousand atomic units before being turned back by the magnetic field. Panel *b* shows the waves returning from the outer zone along classical orbits (4), and entering the inner zone (5), where they overlap with the initial waves to produce modulations in the photoabsorption spectrum. Part of the waves are backscattered by the Coulomb field (6). Panel *c* gives a schematic view of the recoupling when the electron returns into the inner zone: as the electron approaches the core, the wave function, previously described in the uncoupled basis $|N_j m_j\rangle$ is projected onto the coupled basis $|\Lambda\rangle$, in which the projection of the angular momentum on the internuclear axis is well defined. The radius of the outer circle is at about 10 a.u. The core-scattering process is best described in this basis, after which the coupled waves are recombined to give newly outgoing waves (7) described again in the uncoupled basis, where the rotational state of the ionic core is well defined. Panel *d* shows the outgoing waves traveling in the outer region (7) and returning to the core (8), producing additional modulations in the photoabsorption spectrum.

enters the outer region; the wave function is then propagated along classical trajectories; (4) some trajectories return to the core: those trajectories define the primitive or geometric orbits; (5) the Rydberg electron is then again coupled to the molecular core: the returning waves interfere with the initially excited waves to produce modulations in the photoabsorption spectra; (6) the Coulomb field backscatters the returning waves, resulting in repetitions of the primitive orbits; (7) the core scatters the previously returning waves; this quantum multichannel process mixes these waves and gives rise to newly outgoing waves which propagate semiclassically in the outer region; and (8) these waves return once more to the core producing additional modulations in the photoabsorption spectra. The same process is again repeated but each core-scattering event reduces the amplitude of the

modulations and, in the semiclassical, limit additional core scattering becomes negligible.

B. Initial excitation and quantum propagation

The molecule is initially in its ground state, compactly localized in the core region where the magnetic field is negligible. Thus, the ground state is a field-free state $|\psi_0\rangle$ that we assume to have the quantum numbers $\Lambda=0$ (hence, a Σ state), $J=0$ and $l=0$ for the "outer" electron, so that in the molecular frame (coupled basis),

$$|\psi_0\rangle=|\Lambda=0J=0\rangle|l=0\lambda=0\rangle F_{l=0}(r), \qquad (7)$$

where $F_{l=0}(r)$ is the unknown radial function of the "outer" electron. For definiteness, take the laser to be linearly polarized along the (space-fixed) magnetic field axis $\hat{z}$ and let $\mathbf{D}$ be the dipole operator in the space-fixed frame. The photoexcitation takes place in the region near the core and is best described in the molecular frame. As in the atomic case, the resulting outgoing wave is given by $G\mathbf{D}|\psi_0\rangle$ [5] where G is the quantum-mechanical outgoing Green's function, described for the molecular case in Appendix C. Since $|\psi_0\rangle$ is a coupled basis (Born-Oppenheimer) function, the form given in Eq. (C3) is the appropriate choice. The outgoing wave is thus obtained as

$$\psi_{\text{out}}(r)=-2^{5/2}\pi\sum_{j}|j\rangle g_{l_j}^+(r)\sum_{\alpha}e^{i\pi\mu_\alpha}\langle j|\alpha\rangle D_\alpha \qquad (8)$$

with

$$D_\alpha=\int 2^{3/2}r'^3 dr'[(f_{l_\alpha}(r')\cos\pi\mu_\alpha+g_{l_\alpha}(r')\sin\pi\mu_\alpha)$$
$$\times\langle\alpha|]\mathbf{D}[|\Lambda=0J=0\rangle|l=0\lambda=0\rangle F_{l=0}(r')]. \qquad (9)$$

The dipole transition will leave the system in states with $J_\alpha=1$, $l_\alpha=1$ and $\Lambda_\alpha=0$ (Σ state) or $|\Lambda_\alpha|=1$ (Π state) (we have assumed $\Lambda_{\text{core}}=0$, so $\lambda_{\text{electr}}=\Lambda$). Expressing $\mathbf{D}$ in terms of molecule fixed components through the direction cosine matrices [23] and evaluating the rotational parts yields

$$D_\alpha=C_\alpha 3^{-1}\int 2^{3/2}r'^3 dr'[f_{l_\alpha}(r')\cos\pi\mu_\alpha$$
$$+g_{l_\alpha}(r')\sin\pi\mu_\alpha]F_{l=0}(r') \qquad (10)$$

with $C_\alpha=1$ if $|\Lambda_\alpha J_\alpha l_\alpha\rangle=|011\rangle$, $C_\alpha=\sqrt{2}$ if $|\Lambda_\alpha J_\alpha l_\alpha\rangle=|111\rangle$ and $C_\alpha=0$ otherwise.

The excitation process thus restricts the sum over α in Eq. (8) to the only two states for which $C_\alpha\neq 0$. This further has the consequence of restricting the sum over j to the values that yield a nonzero $\langle j|\alpha\rangle$, namely, $|N_jl_jm_j\rangle=|010\rangle$, $|N_jl_jm_j\rangle=|210\rangle$ and $|N_jl_jm_j\rangle=|21\pm1\rangle$. Since the energy partition is

$$E=E_{N_jm_j}^{\text{el}}+N_j(N_j+1)B_r+m_j\gamma/2, \qquad (11)$$

where E^{el} is the energy of the outer electron and B_r the core rotational constant, there are two effective dynamical regimes for the outer electron, each associated with a different rotational state of the core, $N=0$ and $N=2$ (the dependence on m through the Zeeman term for the $N=2$ levels is very small).

C. Semiclassical propagation

When the outgoing waves enter the outer zone, where the magnetic field cannot be neglected, we resort to semiclassical propagation [17]: the wave function is calculated from the properties of the classical trajectories and from the knowledge of the wave function on an initial surface. As in usual closed-orbit theory [5,7], let (r_i,θ_i) define an initial surface. Equation (8) reads, by explicitly writing the indices

$$\psi_{\text{out}}(r_i,\theta_i)=\sum_{N_jm_j}|N_jm_j\rangle$$
$$\times\left[-2^{5/2}\pi\sum_{l_j\geqslant|m_j|}g_{l_j}^+(r_i)Y_{l_jm_j}(\theta_i)\right.$$
$$\left.\times\sum_{\alpha}e^{i\pi\mu_\alpha}\langle j|\alpha\rangle D_\alpha\right], \qquad (12)$$

where the notation $Y_{l_jm_j}(\theta_i)$, standing for $Y_{l_jm_j}(\theta_i,0)$ will be used throughout. An approximate analytic solution may be obtained by using the zero-energy approximation for $g_{l_j}^+(r)$, from which $g_{l_j}^+(r)\rightarrow iH_{2l_j+1}^{(1)}(\sqrt{8r})/\sqrt{8r}$, where $H_{2l_j+1}^{(1)}$ is the Hankel function of the first kind, and the asymptotic approximation for large x of the Hankel function $H_{2l_j+1}^{(1)}(x)$ $\rightarrow(\pi x/2)^{-1/2}\exp[i(x-l_j\pi-3\pi/4)]$. We then write the molecular wave function in the outer zone as

$$\psi(r,\theta)=\sum_{N_jm_j}|N_jm_j\rangle\psi^{N_jm_j}(r,\theta), \qquad (13)$$

where $\psi^{N_jm_j}(r,\theta)$ is the semiclassical wave function associated with the core in state $|N_jm_j\rangle$,

$$\psi^{N_jm_j}(r,\theta)=\sum_{k}\psi_{\text{out}}^{N_jm_j}(r_i,\theta_{ik})\left|\frac{r_i^2\sin\theta_{ik}}{r^2\sin\theta}\right|^{1/2}$$
$$\times A_k^{N_jm_j}(r,\theta)$$
$$\times\exp[i(S_k^{N_jm_j}(r,\theta)-\omega_k^{N_jm_j}\pi/2)]. \qquad (14)$$

A_k and S_k are the classical amplitude and phase functions for trajectory k in the 2 dimensional axial plane, and ω_k is the associated Maslov index. The superscripts N_jm_j on the *classical* quantities determine the energy at which the classical trajectories must be calculated, following the energy partition (11); the value of m_j also affects the counting of z axis crossings in the computation of the Maslov index [4,5].

The wave on the initial surface associated with the core in state $N_j m_j$ is written $\psi_{\text{out}}^{N_j m_j}(r_i, \theta_{ik})$ and given by the term between the square brackets in Eq. (12); it takes the approximate analytic form

$$\psi_{\text{out}}^{N_j m_j}(r_i, \theta_{ik}) = -i\pi^{1/2}2^{3/4}r_i^{-3/4}$$

$$\times \sum_{l \geq |m_j|} (-1)^{l_j} Y_{l_j m_j}(\theta_{ik}) e^{i(\sqrt{8r_i} - 3\pi/4)}$$

$$\times \sum_{\alpha} e^{i\pi\mu_\alpha} \langle N_j l_j m_j | \alpha \rangle D_\alpha. \quad (15)$$

Note that Eqs. (14) and (15) have the same structure as the semiclassical outgoing waves in atomic closed-orbit theory. The overall wave function in the outer zone is a superposition of such wave functions, taken for different dynamical regimes. But, as expected, the classical dynamics of the electron in the outer region does not depend on the presence of the core.

D. Primitive returning waves

1. Returning waves in the inner region

Eventually, some trajectories in the outer region return to the inner region. The wave function in the part of the outer region near the inner region, where the magnetic field is weak, is the one carried by the classical trajectories closed at the origin. It is given by Eqs. (13)–(15), where the sum over k involves the trajectories that return to the inner region. The wave function in the inner region is written as a MQDT expansion in the uncoupled basis, Eq. (B5),

$$\psi^1(r) = \sum_j |j\rangle \sum_{j'} c_{j'} [\delta_{jj'} f_{l_j}(r) + T_{jj'} g_{l_j}^+(r)], \quad (16)$$

where the superscript 1 indicates the first return to the inner region. The coefficients c_j are obtained by matching ψ^1 to Eq. (13). Orthonormality of the core states leads to an independent matching for each $N_j m_j$ subspace. We thus break the radial standing-wave f_{l_j} in Eq. (16) into incoming and outgoing components: following Eq. (B4), we have $f_l = (g_l^+ - g_l^-)/2i$. Hence,

$$\sum_{l_j} -c_{l_j}^{N_j m_j} Y_{l_j m_j}(\theta_f) g_{l_j}^-(r_f)/2i = \psi^{N_j m_j}(r_f, \theta_f), \quad (17)$$

where we have written explicitly $c_j \equiv c_{l_j}^{N_j m_j}$. We now use the orthonormality of the spherical harmonics, to write

$$-c_{l_j}^{N_j m_j} g_{l_j}^-(r_f)/2i = 2\pi \int_0^\pi d\theta_f \sin\theta_f Y_{l_j m_j}^*(\theta_f) \psi^{N_j m_j}(r_f, \theta_f), \quad (18)$$

and perform the integration for each trajectory k using the stationary phase approximation along the angle of stationary phase. Proceeding as in [12], we write the action at (r_f, θ_f) for the kth trajectory as $S_k^{N_j m_j}(r_f, \theta_f) = S_{k(\text{closed})}^{N_j m_j}$

$-\sqrt{8r_f} \cos[(\theta_f - \theta_{fk})/2]$, where $S_{k(\text{closed})}^{N_j m_j}$ is the action of the kth trajectory closed at the origin. The angle of stationary phase is then simply θ_{fk} and the stationary phase integration leads to

$$-c_{l_j}^{N_j m_j} g_{l_j}^-(r_f)/2i = \frac{2\pi(2\pi\hbar)^{1/2}e^{i\pi/4}}{2^{-1/4}r_f^{1/4}}$$

$$\times \left\{ \sum_k Y_{l_j m_j}^*(\theta_{fk}) r_i r_f^{-1} \right.$$

$$\times |\sin\theta_{ik} \sin\theta_{fk}|^{1/2} A_k^{N_j m_j}(r_f, \theta_{fk})$$

$$\times \exp[i(S_{k(\text{closed})}^{N_j m_j} - \sqrt{8r_f} - \sqrt{8r_i}$$

$$\left. - \omega_k^{N_j m_j}\pi/2)]\psi_{\text{out}}^{N_j m_j}(r_i, \theta_{ik}) \right\}. \quad (19)$$

Choosing $r_f = r_i$, using the zero-energy approximation $g_{l_j}^-(r) \rightarrow -iH_{2l_j+1}^{(2)}(\sqrt{8r})/\sqrt{8r}$, where $H_{2l_j+1}^{(2)}$ is the Hankel function of the second kind, together with the asymptotic approximation to $H_{2l_j+1}^{(2)}$, we obtain our final expression for the coefficients

$$c_{l_j}^{N_j m_j} = \hbar^{1/2}2^{3/2}2^3\pi^2 r_f^{1/2}e^{-i\pi/2}\left\{ \sum_k Y_{l_j m_j}^*(\theta_{fk}) \right.$$

$$\times (-1)^{l_j+1}|\sin\theta_{ik}\sin\theta_{fk}|^{1/2}A_k^{N_j m_j}(r_f, \theta_{fk})$$

$$\times \exp[i(S_{k(\text{closed})}^{N_j m_j} - \sqrt{8r_f} - \omega_k^{N_j m_j}\pi/2)]$$

$$\left. \times \psi_{\text{out}}^{N_j m_j}(r_i, \theta_{ik}) \right\}. \quad (20)$$

2. Contribution to the oscillator strength

These primitive returning waves contribute to the oscillatory part of the oscillator strength through the imaginary part of $\langle D\psi_0 | G^+ | D\psi_0 \rangle$ [5] which we rewrite here as $\langle \psi_0 | \mathbf{D} | \psi^1 \rangle$, i.e., the overlap of the initially excited waves with the returning waves. Following the same arguments given in Sec. III B, in order to calculate the dipole transition, ψ^1 must be written in the coupled frame. Using Eqs. (B3) and (B4), we have

$$\psi^1(r) = \sum_\alpha |\alpha\rangle c_\alpha e^{i\pi\mu_\alpha}[f_{l_\alpha}\cos\pi\mu_\alpha + g_{l_\alpha}\sin\pi\mu_\alpha], \quad (21)$$

where the expansion coefficients c_α are obtained from the coefficients c_j of Eq. (20) via the frame transformation (B7). c_α represents the weight of the returning waves coming along all the trajectories k closed at the origin (and for all of the allowed dynamical regimes of the Rydberg electron, indexed by $N_j m_j$) that find themselves recombined in the coupled channel α. This recombination depends both on the characteristics of the classical trajectories and those of the quantum transformation coefficients. Using Eq. (9), we express the overlap as

$$\langle \psi_0 | \mathbf{D} | \psi^1 \rangle = \sum_\alpha c_\alpha e^{i\pi\mu_\alpha} 2^{-3/2} D_\alpha^* . \qquad (22)$$

This expression is evaluated by expanding the coefficients c_α in terms of the c_j and by using the united atom approximation. This approximation consists of setting the radial integral appearing in Eq. (10) to some unknown value *independent* of α. We thus determine relative oscillator strengths and accordingly replace D_α by C_α (the united atom approximation is known from field-free experiments to be adequate for H_2; in the general case, relations between the radial integrals for different values of α may be extrapolated from field-free *ab initio* calculations or from experimental data).

The final result is

$$\langle \psi_0 | \mathbf{D} | \psi^1 \rangle = \hbar^{1/2} 2^{15/4} \pi^{5/2}$$

$$\times \sum_j \left\{ \sum_{\alpha,\alpha'} \langle j | \alpha' \rangle \langle \alpha | j \rangle C_\alpha C_{\alpha'} e^{i\pi(\mu_\alpha + \mu_{\alpha'})} \right\}$$

$$\times \sum_k \mathcal{R}_k^j \qquad (23)$$

with

$$\mathcal{R}_k^j = |\sin\theta_{ik} \sin\theta_{fk}|^{1/2} r_f^{-1/4} A_k^{N_j m_j}(r_f, \theta_{fk})$$

$$\times \exp[i(S_{k(\text{closed})}^{N_j m_j} - \omega_k^{N_j m_j} \pi/2 - 3\pi/4)]$$

$$\times \sum_{l_j \geqslant |m_j|} \sum_{l_{j'} \geqslant |m_{j'}|} (-1)^{l_{j'}} Y_{l_{j'} m_{j'}}(\theta_{ik})$$

$$\times (-1)^{l_j} Y_{l_j m_j}^*(\theta_{fk}). \qquad (24)$$

Note that, for the orbit along the magnetic field axis with $\theta_{ik} = \theta_{fk} = 0$, $\mathcal{R}_k^j$ as given by Eq. (24) is identically zero and must be modified following the prescription given in Appendix D.

The imaginary part of Eq. (23) gives the sinusoidal modulations contributed by each orbit k of the electron associated with a given state $N_j m_j$ of the core. In the present model the sum over j runs over the four allowed core states and $l=1$. For $N=2$ $m=0,\pm 1$ the actions are smaller and the resulting modulations are larger than for the orbits associated with $N=0$ $m=0$. Note that the contributions of the classical orbits for the different values of j are combined through the term between braces which reflects the inner-region quantum dynamics.

E. Core-scattered outgoing waves

The outgoing part of $\psi^1(r)$ [Eq. (16)] contains two different terms. First, the wave scattered by the Coulomb field, composed from the outgoing parts of f_{l_j}; on the boundary radius, we have $g_{l_j}^+(r_f) \approx -e^{2i\sqrt{8r_f}} e^{-3i\pi/2} g_{l_j}^-(r_f)$, so taking into account the increase of the Maslov index by one at the origin, the Coulomb scattered waves are simply given by $e^{2i\sqrt{8r_f}} e^{-i\pi} \psi^{N_j m_j}(r_f, \theta_f)$: as in atomic closed-orbit theory [7] these waves are strongly backward focused, retracing the

original orbits in reverse without changing the state of the core. Their contribution to the modulations of the photoabsorption spectra is taken into account by keeping track of the orbit repetitions and we shall not be concerned by these waves in what follows.

The second term, namely,

$$\psi_{\text{core}}^1(r,\theta) = \sum_{N_j m_j} |N_j m_j\rangle \sum_{l_j} Y_{l_j m_j}(\theta) g_{l_j}^+(r) \sum_{j'} c_{j'} T_{jj'}, \quad (25)$$

represents the core-scattered waves: each newly outgoing wave leaving the core in state $|N_j m_j\rangle$ results from the scattering into channel j from waves that previously returned into channel j', i.e., with the core being in a state $|N_{j'} m_{j'}\rangle$. These interchannel mixings are formally represented by the T-matrix elements.

These outgoing waves leave the inner region and propagate semiclassically in the outer region. The procedure described in Sec. III C is now applied to Eq. (25). We have in the outer region

$$\psi_{\text{core}}^1(r,\theta) = \sum_{N_j m_j} |N_j m_j\rangle \psi_{\text{core}}^{N_j m_j}(r,\theta) \qquad (26)$$

with

$$\psi_{\text{core}}^{N_j m_j}(r,\theta) = \sum_q \left[i\pi^{-1/2} 2^{-7/4} r^{-3/4} e^{i(\sqrt{8r_i} - 3\pi/4)} \right.$$

$$\times \sum_{j'} c_{j'} T_{jj'} \sum_{l_j \geqslant |m_j|} Y_{l_j m_j}(\theta_{iq})(-1)^{l_j} \Bigg]$$

$$\times \left| \frac{r_i^2 \sin\theta_{iq}}{r^2 \sin\theta} \right|^{1/2} A_q^{N_j m_j}(r,\theta) \exp[i(S_q^{N_j m_j}(r,\theta)$$

$$- \omega_q^{N_j m_j} \pi/2)]. \qquad (27)$$

Some trajectories q eventually return to the core, and the returning wave is matched to a MQDT expansion analog to Eq. (16),

$$\psi^2(r) = \sum_j |j\rangle \sum_{j'} d_{j'} [\delta_{jj'} f_{l_j}(r) + T_{jj'} g_{l_j}^+(r)], \quad (28)$$

where the superscript 2 stands for the second return to the inner region. The coefficients d_j are obtained by matching this expansion to the semiclassical returning waves [cf. Eqs. (17)–(20)]. Note that d_j, similar to Eq. (20) with $\psi_{\text{out}}^{N_j m_j}$ replaced by the term between brackets in Eq. (27), contains terms of the form

$$\sum_{k,q} A_q^{N_j m_j} \exp[i(S_q^{N_j m_j} - \omega_q^{N_j m_j} \pi/2)]$$

$$\times A_k^{N_{j'} m_{j'}} \exp[i(S_k^{N_{j'} m_{j'}} - \omega_k^{N_{j'} m_{j'}} \pi/2)], \quad (29)$$

which clearly combine a classical trajectory k associated with a core in state $|N_{j'} m_{j'}\rangle$ and a trajectory q associated with a core in state $|N_j m_j\rangle$.

The contribution to the oscillator strength is given by the overlap of these returning waves with the initially excited waves,

$$\langle \psi_0 | \mathbf{D} | \psi^2 \rangle = \sum_\alpha d_\alpha e^{i\pi\mu_\alpha} 2^{-3/2} D_\alpha^*, \tag{30}$$

which may be written in terms of c_j and takes the form

$$\langle \psi_0 | \mathbf{D} | \psi^2 \rangle = \sum_{j,j'} \sum_{\alpha,\alpha'} \langle j' | \alpha' \rangle \langle \alpha | j \rangle C_\alpha C_{\alpha'} e^{i\pi(\mu_\alpha + \mu_{\alpha'})}$$

$$\times \left[\hbar^{1/2} 2^{15/4} \pi^{5/2} \sum_k \mathcal{R}_k^{j'} \right]$$

$$\times \left[\hbar^{1/2} 2^{11/4} \pi^{3/2} T_{jj'} \sum_q \mathcal{R}_q^j \right], \tag{31}$$

where the classical quantities $\mathcal{R}$ are given by Eq. (24) and, as explained above, must be modified when $\theta = 0$ or π following the prescription given in Appendix D. The sum over the closed classical orbits contains implicitly a sum over the repetitions. The last bracket (with the trajectories labeled q) represents the orbits consecutive to core scattering and are accordingly weighted by the quantum scattering matrix element $T_{jj'}$, the transition amplitude connecting the waves which originally enter from channel j' and leave in channel j. Hence, Eq. (31) takes into account both elastic ($E_j = E_{j'}$) and inelastic ($E_j \neq E_{j'}$) scattering, and vanishes if there is no core scattering. Note that in the case of single-channel scattering, Eq. (31) reduces to the one core-scatter approximation obtained in the atomic case [13].

Note also that further iterations may be taken into account if necessary: the waves that return to the inner region for the second time are scattered by the core, and produce newly outgoing waves given by $\Sigma_j | j \rangle \Sigma_{j'} d_{j'} T_{jj'} g_{l_j}^+(r)$. These waves propagate in the outer region; Eq. (26) holds for $\psi_{\text{core}}^2(r,\theta)$ provided the coefficients c_j in Eq. (27) are replaced by the d_j's, and the eventually returning waves are matched to a new MQDT expansion with coefficients e_j.

F. Scaled energy spectra

1. Scaling the rotational constant

As in the case of nonhydrogenic Rydberg atoms, the semiclassical formulas derived above only contain the classical trajectory parameters corresponding to the *hydrogenic* case. Hence, the scaling transformations for a hydrogenic electron in a magnetic field, given in Appendix A, were employed, leading to calculations at some fixed value of the scaled energy $\epsilon = E\gamma^{-2/3}$ with an effective Planck constant $\hbar_{\text{eff}} = \gamma^{1/3}\hbar$. From Eq. (11), it is clear that the present problem does not yield an exact scaling property; multiplying both terms of the equation by $\gamma^{-2/3}$ and neglecting the Zeeman shift leads to

$$\epsilon_{N=0} = \epsilon_{N_j} + \gamma^{-2/3} B_r N_j (N_j + 1). \tag{32}$$

Thus, if for example the classical dynamics of the electron associated with the core in state $N=0$ is kept fixed (i.e., $\epsilon_{N=0}$ is constant), the classical dynamics of the electron associated with the core in state $N=2$ will vary with $\gamma^{-2/3}$, thereby encompassing different classical regimes.

If we now set $\tilde{B}_r = \gamma^{-2/3} B_r$ to be a constant, Eq. (32) reads $\epsilon_{N=0} = \epsilon_{N_j} + \tilde{B}_r N_j (N_j + 1)$ resulting in simultaneous scaling of the various classical dynamics of the electron. This procedure amounts to introducing in our calculations an artificial $\gamma^{2/3}$ dependence of the rotational constant. Indeed, if the scaled spectrum is calculated in an interval $[\gamma_1^{-1/3}, \gamma_2^{-1/3}]$ with the midpoint $\gamma_{\text{mid}}^{-1/3} = \frac{1}{2}(\gamma_1^{-1/3} + \gamma_2^{-1/3})$, we set

$$B_r(\gamma) = \gamma_{\text{mid}}^{-2/3} \gamma^{2/3} B_r, \tag{33}$$

where $B_r(\gamma)$ is the rotational "constant" for our model which coincides with the physical rotational constant B_r for $\gamma^{-1/3} = \gamma_{\text{mid}}^{-1/3}$, and which has the important property of yielding a fixed value of the "scaled rotational constant," $\tilde{B}_r = \gamma^{-2/3} B_r(\gamma)$. The consequences of such a choice will be discussed in Sec. VI. We note, however, that the use of scaling techniques in molecular systems, which typically have a nonscaling Hamiltonian, has been advocated [24] as an efficient manner of extracting the underlying classical motion that appears in quantum spectra.

2. Scaled absorption rate

The rate of production of excited molecules is given by a smooth background plus oscillatory contributions. The oscillating part of the absorption rate, $\mathcal{F}(\gamma, \epsilon)$, is related to the oscillator strength of Eq. (1) by [8]

$$\mathcal{F}(\gamma, \epsilon) = \gamma^{-1/6} \frac{f_1(\gamma, \epsilon)}{E - E_0}. \tag{34}$$

At fixed values of ϵ, this reduced absorption rate reads

$$\mathcal{F}(\hbar_{\text{eff}}) = \frac{2}{\pi \hbar_{\text{eff}}^{1/2}} \sum_P \text{Im}[\langle \psi_0 | \mathbf{D} | \psi^P \rangle], \tag{35}$$

where P counts the number of returns to the core region. For example, taking into account only terms up to $P=2$ gives [Eqs. (23) and (31)]

$$\mathcal{F}(\hbar_{\text{eff}}) = 2^{19/4} \pi^{3/2} \sum_j \sum_\alpha \sum_{\alpha'} \text{Im}\left\{ \langle \alpha | j \rangle C_\alpha C_{\alpha'} e^{i\pi(\mu_\alpha + \mu_{\alpha'})} \right.$$

$$\times \left[\langle j | \alpha' \rangle \sum_k \tilde{\mathcal{R}}_k^j + \hbar_{\text{eff}}^{1/2} 2^{11/4} \pi^{3/2} \right.$$

$$\left. \times \sum_{j'} \langle j' | \alpha' \rangle T_{jj'} \sum_k \tilde{\mathcal{R}}_k^{j'} \sum_q \tilde{\mathcal{R}}_q^j \right] \right\} \tag{36}$$

where the factors $\tilde{\mathcal{R}}_k^j$ are now written in terms of the scaled classical variables $\tilde{S}_k^j = \hbar_{\text{eff}} S_k^j / 2\pi\hbar$ and $\tilde{r}_f^{-1/4} A_k^j = |2^{1/2} \cos(\theta_{ik}/2) \cos(\theta_{fk}/2) m_{12}|^{-1/2}$ where m_{12} is an element

of the 2×2 stability matrix evaluated in the scaled semiparabolic coordinate system (see Appendix D).

IV. QUANTUM CALCULATIONS

We calculated a set of quantal eigenvalues and eigenstates for the scaled molecule, corresponding to scaled energy $\epsilon = -0.3$ in the $N=0$ channel and $\epsilon = -0.8$ in the $N=2$ channels. These were then Fourier transformed and compared with the equivalent spectral range in the semiclassical calculations.

The method employed is similar to that used previously for *unscaled* calculations of Rydberg H_2 in a field by He *et al.* [21]. The Schrödinger equation, in an outer-region $r_0 \leq r \leq \infty$ where short-ranged interactions with the core may be neglected, is

$$\hat{H}_o \psi_n = \left\{ -\frac{1}{2}\nabla^2 - \frac{1}{r} + \frac{1}{8}\gamma^2 \rho^2 + B_r \hat{N}^2 + \gamma L_z \right\}\psi_n = E_n \psi_n .$$
(37)

In Ref. [21], the solutions were expanded in the uncoupled basis $|j\rangle = |Nlm\rangle = Y_{lm}(\hat{\boldsymbol{r}})Y_{NM-m}(\hat{\boldsymbol{R}})$ (we drop the subscripts if they are not necessary) with the radial part of the wave function described in a basis of Sturmian functions

$$\psi_n(\boldsymbol{r},\boldsymbol{R}) = \sum_{Nlm} C_n^{Nlm} \frac{S_{nl}^\zeta}{r}|Nlm\rangle,$$
(38)

and the outer-region Hamiltonian $\hat{H}_o$ was then diagonalized in the uncoupled basis with an additional surface term, i.e.,

$$\langle \psi_{n'}|\hat{H}_o + \hat{L}|\psi_n\rangle = E_n \delta_{nn'} .$$
(39)

The surface operator is known in terms of the molecular basis $|\Lambda Jl\rangle = |\alpha\rangle$,

$$\hat{L} = -\sum_\alpha |\alpha\rangle \delta(r-r_0)\left(\frac{\partial}{\partial r} - B_\alpha\right)\langle\alpha|.$$
(40)

The first term $\delta(r-r_0)\partial/\partial r$ is a Bloch term which is necessary because the d^2/dr^2 operator is not Hermitian over the limited range $r_0 \leq r < \infty$. The B_α [10] are logarithmic derivatives given in terms of the MQDT wave functions, i.e., $B_\alpha(E_n,r) = P'(E_n,r)/P(E_n,r)$ where $P(E_n,r) = f_{l_\alpha}(r) - \tan(\pi\mu_{\Lambda_\alpha})g_{l_\alpha}(r)$ with f and g denoting the regular and irregular Coulomb functions, respectively. While we do not have the exact logarithmic derivatives $B_\alpha(E_n,r)$ one can exploit their relative insensitivity to energy. A value for the logarithmic derivative at some reference energy $B_\alpha(E = E_0,r)$ is used to obtain good approximations to a few eigenvalues with energies close by $E \simeq E_0$. The reference energy is then adjusted and the next band of energies is obtained: and so forth, until the desired stretch of eigenvalues and corresponding eigenvectors has been obtained. This procedure, combined with the efficient Lanczos algorithm which computes only a few neighboring eigenvalues of the Hamil-

tonian matrix at each reference energy, was used successfully in Ref. [10] to study the spectra of nonhydrogenic atoms in fields.

This method was adapted here for the corresponding *scaled* molecule in a magnetic field. With rescaled position coordinates (see Appendix A) the corresponding outer-region Schrödinger equation may be rearranged to take the form

$$\left\{ -\frac{1}{r} + \frac{1}{8}r^2\sin^2\theta + \epsilon_{Nm} - \epsilon \right\}\psi_n = \frac{\gamma_n^{2/3}}{2}\{\nabla^2 - \hat{L}\}\psi_n .$$
(41)

The ϵ_{Nm} are the scaled channel energies explained in Sec. III F above. This solution of the equation now represents a generalized eigenvalue problem with the magnetic fields $\gamma_n^{2/3}$ corresponding to a set of fixed scaled energies in every channel and $\gamma_n^{1/3}$ plays the role of an effective Planck's constant.

In our calculations, we allowed ten channels ($N=0,2,4,6$ with three Zeeman components in the $N>0$ channels). However the contribution from the $N=4$ and $N=6$ states (which were relatively few in number) is small. It was found that adjusting the exponent on the Sturmian basis for each channel, i.e., $S_{nl}^{\zeta_{Nm}}(r)$ was essential for an efficient calculation. Since the $N>0$ states correspond to low-principal quantum numbers, a much smaller basis could be used. So although we have ten channels, the Rydberg molecule calculations involve matrices only two or three times larger than an equivalent calculation for a Rydberg *atom* in an external magnetic field.

V. RESULTS

A. Introductory remarks

We compare below the semiclassical calculations, obtained by following the theory detailed in Sec. III, to exact quantum results obtained by R-matrix calculations as outlined in Sec. IV. Previously [22], we have found a reasonable agreement between semiclassical and quantum calculations in the case of H_2 and its isotopomers (the figures shown in [22] were for T_2).

However, an appropriate comparison between semiclassical and quantum calculations (avoiding the appearance of purely quantum effects) requires the dynamics of the outer electron to have attained the semiclassical limit in both rotational channels. As implied by Eqs. (11) and (32), the effective quantum number of the $N=2$ Rydberg series decreases with an increasing rotational constant B_r. So when B_r increases, lower energies are obtained in the $N=2$ channels for a fixed value of the scaled energy $\epsilon_{N=0}$. We chose $\epsilon_{N=0} = -0.3$ because recurrence spectra for hydrogen and nonhydrogenic Rydberg atoms for that particular value $\epsilon = -0.3$ have been extensively investigated. However, in order to compare quantum and semiclassical results, the scaled quantum calculations for a molecule need to be performed for higher values of the effective quantum number (for the same value of the scaled energy in the $N=0$ rotational channel) than for an atom. This requires increasing basis sizes, CPU time and computer resources. For H_2, the value of the rota-

tional constant, $B_r \simeq 1.33 \times 10^{-4}$ a.u. is particularly large, so obtaining appropriate quantum calculations for a detailed comparison with the semiclassical calculations is prohibitively expensive.

To assess the validity of the semiclassical formalism vis-à-vis exact quantum mechanics, we have chosen instead to investigate a model molecule with a smaller rotational constant, thereby reducing the gap between the energies of the electron associated with the different rotational channels. We compare below the results for $M=0$, in a magnetic field range $\gamma^{-1/3} = 60-120$ at constant scaled energies $\epsilon_{N=0} = -0.3$ and $\epsilon_{N=2} = -0.8$ (equivalent to choosing $B_r(\gamma_{\mathrm{mid}}^{-1/3} = 90)$ about four times smaller than the rotational constant of T_2). Note that from a qualitative standpoint, the classical dynamics of the electron is not modified for larger choices of B_r: indeed, this would only bring in lower values of $\epsilon_{N=2}$, and it is well-known that, even at $\epsilon = -0.8$, the classical dynamics remains very close to its integrable limit $\epsilon \rightarrow -\infty$.

B. Recurrence spectra

Figure 2 displays the Fourier transform of the oscillatory part of the photoabsorption spectra for different choices of the quantum defects μ_Σ and μ_Π. As usual, the smooth background term has been subtracted before taking the Fourier transform of the quantum spectra, whereas the semiclassical recurrence spectra were obtained by taking the Fourier transform of Eq. (36), thus including one core scattering. Equation (36) is of course proportional to the imaginary part of Eqs. (23) and (31), which will prove more useful in the analysis of the present results. Since the intensities are only defined to an overall constant, the quantum and semiclassical Fourier spectra were renormalized, usually by adjusting the amplitude of the peak at scaled action $\tilde{S} = 1.26$ [labeled 1 in Fig. 2(a)]. The main peaks in Fig. 2 are numbered. The classical closed orbits that contribute to the semiclassical spectra are plotted in (ρ, z) coordinates in Fig. 6 in Appendix D while Table I lists the scaled action and amplitude for the first returns to the nucleus of each of the orbits and identifies the numbered peaks at which the orbit and its repetitions contribute; the correspondence with the orbit labeling convention introduced in Ref. [29] is also given.

In the case of zero quantum defects [Fig 2(a)], the T matrix vanishes and there is no core scattering: the resulting spectrum is identical to the one obtained in the case of the hydrogen atom at $\epsilon = -0.3$, which has been extensively investigated and discussed thoroughly (see [8] and references therein). The absence of any features related to the dynamics of the electron associated with the rotationally excited states of the core is evident. This is always the case when $\mu_\Sigma = \mu_\Pi$: the sum over α in Eq. (8) cancels for $N_j = 2$, and thus no electron associated with an $N=2$ core is excited by the laser field. Further, for $\mu_\Sigma = \mu_\Pi$ nonzero, the T matrix, given by Eq. (B6), is diagonal and accordingly only the terms with $N_j = N_{j'} = 0$ survive in Eq. (31). Put differently, there is no rotational interaction, and thus only elastic core scattering is expected. In this case, the molecule behaves in a quasiatomic manner. This is seen in Fig. 2(b) for the quantum defects $\mu_\Sigma = \mu_\Pi = 0.5$; the additional peaks, not present in Fig. 2(a),
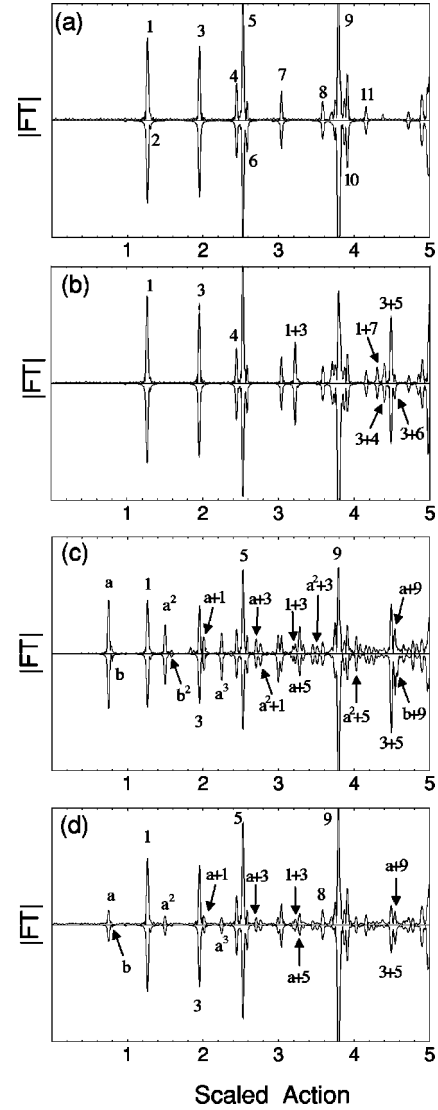

FIG. 2. Recurrence spectra for molecules with different quantum defects at scaled energies $\epsilon_{N=0} = -0.3$ (predominantly chaotic phase space) and $\epsilon_{N=2} = -0.8$ (near integrable phase space). Within each panel, *quantum* calculations are displayed on top and *semiclassical* calculations upside down. The main peaks are indicated with numbers corresponding to the classical hydrogenic orbits given in Appendix D, or to a combination of those orbits via core scattering. (a) $\mu_\Sigma = 0$, $\mu_\Pi = 0$: only the hydrogenic orbits associated with the core in state $N=0$ appear in the recurrence spectrum. (b) $\mu_\Sigma = 0.5$, $\mu_\Pi = 0.5$: new peaks associated with the core in state $N=0$ are visible; these peaks are produced by *elastic* core scattering. (c) $\mu_\Sigma = 0.5$, $\mu_\Pi = 0$: additional peaks are visible; these new peaks correspond (i) to the hydrogenic orbits associated with the core in state $N=2$ (labeled a $[m=\pm 1]$ and b $[m=0]$) and (ii) to peaks produced by *inelastic* core scattering, combining hydrogenic orbits belonging to the different classical regimes. (d) $\mu_\Sigma = 0.22$, $\mu_\Pi = -0.06$: these are the approximate values of the quantum defects of the ungerade $l=1$ complex of H_2 at equilibrium internuclear distance; as in (c), all types of orbits (hydrogenic orbits of the electron associated with the core in states $N=0$ and $N=2$ $m=0,\pm 1$, elastic and inelastic core-scattered orbits) are visible, but with different relative amplitudes.

TABLE I. Scaled action and amplitude of the classical closed orbits contributing to the semiclassical spectra at $\epsilon=-0.3$, and $\epsilon=-0.8$. The key A–U is used to identify the orbits with the trajectory plots displayed in Fig. 6. The peak label, corresponding to the numbers used in Figs. 2 and 4, denotes the peaks in the spectra to which each of the orbits and their repetitions contribute. Note that the multiple entries for the amplitude and peak label for orbits B, C, and D correspond to the contributions from the first, second, and third repetitions, respectively, of those orbits. The orbit label identifies the orbit, where possible, with the familiar naming scheme introduced in Ref. [29].

		$\epsilon=-0.3$		
Key	Action	Amplitude	Peak Label	Orbit Label
A	0.9753	0.6325		R_1
B	1.2636	0.2015, 0.1504, 0.1352	1, 5, 9	V_1^1
C	1.2910	0.4894, 1.1183, 0.6054	2, 6, 10	V_1
D	1.9541	0.6065, 0.4011	3, 10	R_2^1
E	2.4444	0.1247	4	V_2^1
F	2.5323	0.1125	5	V_2^{2*}
G	3.0389	0.1179	7	R_3^1
H	3.5862	0.0679	8	V_3^1
I	3.7486	0.0555		V_3^2
J	3.7917	0.1315	9	
K	3.7941	0.1199	9	
L	3.7944	0.1409	9	
M	3.8150	0.0462		
N	3.8723	0.0437	10	V_3^4
O	4.1575	0.0526	11	R_4^1
P	4.7171	0.0349		V_4^1
Q	4.9036	0.0327		
R	4.9743	0.0450		
S	4.9753	0.0391		
T	4.9856	0.0942		
U	4.9893	0.0934		
		$\epsilon=-0.8$		
	Action	Amplitude	Peak Label	Orbit Label
	0.7487	12.7988	a	R_1
	0.7906	11.9017	b	V_1

correspond to a combination of orbits associated with the ground $N=0$ core state (e.g., the peak at $\widetilde{S}=3.21$, which is the combination of the hydrogenic orbits 1 at $\widetilde{S}=1.26$ and 3 at $\widetilde{S}=1.95$). These additional peaks were observed in the case of nonhydrogenic Rydberg atoms with a quantum defect $\mu=0.5$ [13]. Note that the semiclassical calculation is in excellent agreement with the quantum results.

Figures 2(c) $[\mu_\Sigma=0.5, \mu_\Pi=0]$ and 2(d) $[\mu_\Sigma=0.22, \mu_\Pi=-0.06]$ display a far greater number of peaks, characteristic of a more realistic molecular situation. First of all, peaks corresponding to contributions from the orbits associated with an excited core corresponding to a classical dynamics at scaled energy $\epsilon_{N=2}=-0.8$ are clearly visible. The shortest of these orbits gives rise to the peak labeled a at $\widetilde{S}=0.75$. It is an orbit perpendicular to the field axis ($\theta_i=\theta_f=\pi/2$) and is associated with the $N=2$, $m=\pm1$ submanifold of the rotationally excited states, since the factor $\mathcal{R}_k^j$ given by Eq. (23) vanishes for this orbit when $m=0$. Next to it, the peak b at $\widetilde{S}=0.79$, which appears with a far smaller amplitude, corresponds to an orbit parallel to the

field ($\theta_i=\theta_f=0$); it is associated with the $N=2$, $m=0$ core state. The repetitions of these orbits (the first of which are at $\widetilde{S}=1.50$ and 1.58, respectively) are clearly visible. The peaks corresponding to orbits associated with the $N=0$ ground state are also readily identified [e.g., by comparison with Figs. 2(a) and 2(b)]; each of these involve both the hydrogenic and the core-scattered orbits. Furthermore, there are peaks appearing at a scaled action corresponding to the sum of an $\epsilon_{N=0}$ orbit and an $\epsilon_{N=2}$ orbit. For example, the peak at $\widetilde{S}=2.01$ arises from the combination of the "balloon" V_1^1 orbit (peak 1) at scaled energy $\epsilon_{N_j=0}=-0.3$ and action $\widetilde{S}_k=1.26$ with the perpendicular R_1 orbit (peak a) at scaled energy $\epsilon_{N_{j'}=0}=-0.8$, and action $\widetilde{S}_q=0.75$ (and it is accordingly labeled a+1). From a physical standpoint, the resulting peak is produced by inelastic scattering: the electron along an orbit k with the core in state j collides with the core, exchanging energy and leaving the core in state j' along an orbit q, as predicted by Eq. (31).

Hence, the vast majority of the peaks appearing in the quantum recurrence spectra of Figs. 2(c) and 2(d) are ex-

plained semiclassically as resulting from primitive, elastic, and inelastic core-scattered orbits. Furthermore, our semiclassical theory is seen to yield a good quantitative agreement with the exact quantum calculations. Equation (23) indicates how the relative amplitude of the peaks corresponding to the primitive orbits associated with the core in states $N=0$ and $N=2$ depends on the short-range quantum defects. Equation (31) shows the dependence of the elastic and inelastic peak heights on the value of the quantum defects: indeed, the amplitude of a core-scattered peak depends both on the classical properties of the orbits, contained in the factors $\mathcal{R}$, and on the purely quantal scattering matrix amplitudes $T_{jj'}$. Note also that different orbits or combination of orbits having the same total scaled action will interfere, adding constructively or destructively as a function of their relative phase, which contains terms having a classical and a quantum origin. All these effects combine to give the different recurrence spectra displayed in Fig. 2.

C. Higher-order effects

Closed-orbit theory—as with any semiclassical formalism—fails when the classical parameters become singular, for example, near bifurcations, where newly created orbits are born, the stability matrix element $m_{12} \to 0$, and the amplitude of the corresponding orbit is overestimated [see Eqs. (D1) and (D2)]. This is seen in Fig. 2 for the peak labeled 9 at $\tilde{S} = 3.79$ where the semiclassical amplitude is overestimated, due to the existence of a period-three bifurcation of V_1^1 at a slightly lower-scaled energy $\epsilon = -0.3184$ [25]. Note that the semiclassical amplitude of a peak produced by core scattering with a hydrogenic peak that is overestimated will likewise be overestimated [e.g., the peak a+9 in Fig. 2(c)]. Such failures of semiclassical formulas are generally repaired by resorting to uniform approximations, and this has been investigated for closed-orbit theory by Main and Wunner [26]. Here we shall mention two other effects that appear at higher orders of $\hbar$ and that account for some of the discrepancy between our quantum and semiclassical results.

1. Semiclassically forbidden orbits

From the formulas given in Sec. III, it is apparent that some classically existing closed orbits that might have a large amplitude will nevertheless not contribute to the recurrence spectrum. For instance, when the initially excited waves propagate in the outer region or return to the inner region, Eq. (24) asserts that if the initial or final angle of trajectory k lies along a node of the wave function, then $\mathcal{R}_k$ vanishes [because $Y_{lm}(\theta_{ik})$ or $Y_{lm}(\theta_{fk})$ vanishes]. However, we have observed the manifestation of such orbits in the quantum spectra. We have plotted in Fig. 3 quantum and semiclassical recurrence spectra with $\mu_\Sigma = 0.5$, $\mu_\Pi = 0.5$, showing the peak at scaled action $\tilde{S} = 1.95$. The dotted line is obtained by Fourier transforming the semiclassical spectra obtained with the "standard" formula Eq. (36). However, we know from classical calculations that at $\epsilon = -0.3$, $\tilde{S} = 1.95$ is the scaled action of the second return of the perpendicular orbit R_1. Although R_1 which has a scaled action $\tilde{S} = 0.975$
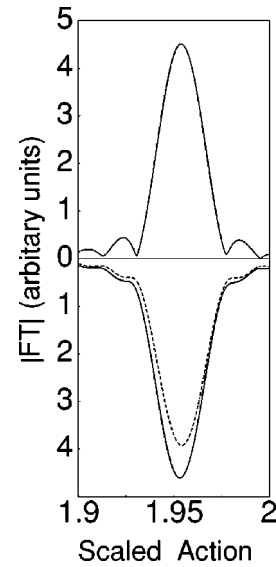

FIG. 3. An enlarged view of the peak at $\tilde{S} = 1.95$ in the recurrence spectrum with $\mu_\Sigma = 0.5$, $\mu_\Pi = 0.5$ [peak labeled 3 in Fig. 2(b)] is shown. Top: quantum result. Bottom: the dashed curve gives the standard closed-orbit result, in which only the R_2^1 orbit contributes to the recurrence spectrum; the solid line includes the contribution of the perpendicular orbit lying on the node of the wave function, which results in a constructive interference. The solid line is in excellent agreement with the quantum calculation.

has a small amplitude, its second and fourth repetitions have a very large amplitude (see the suggestive Fig. 12 of [8]); the same type of mismatch is actually observed at $\tilde{S} = 3.9$, on the fourth return of the perpendicular orbit. But since for the perpendicular orbit $\theta_i = \theta_f = \pi/2$, Y_{10} vanishes and this orbit does not contribute to the spectrum according to the "standard" semiclassical formula.

The contribution of orbits lying in the node of a wave function was observed in the comparison of quantum and semiclassical calculations for the hydrogen atom in a magnetic field [27], and a quantitative formula was given; the contribution of those orbits was found to be extremely small. Such contributions also arise in the spectra of nonhydrogenic atoms and the present results indicate that the resulting effect must be stronger than in hydrogen. The inclusion of these forbidden orbits leads to an improved agreement with the quantum calculations (solid line in Fig. 3). The reason was already put forward by Shaw et al. [27]: an orbit closed at the core is not isolated, but has neighboring orbits (which are not closed at the origin). The contribution of these orbits compared to the central one is usually negligible. However, here the central perpendicular orbit lies on a node of the initial outgoing wave function so the semiclassical wave function can only be carried by the neighboring trajectories. At $\epsilon = -0.3$, a strong focusing effect is produced on the second and fourth closures of the central orbit, bringing together near the core region all the neighboring trajectories. Hence, although the contribution of the neighboring orbits is suppressed by a factor $\hbar$ relative to the other contributions, it is still sufficiently strong at $\hbar_{eff} \sim 1/90$ so as to be clearly visible in the recurrence spectra. The method used to obtain the
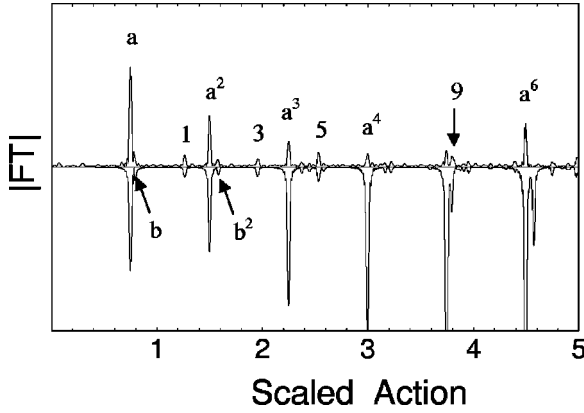
FIG. 4. Recurrence spectrum as in Fig. 2, but for the quantum defects $\mu_\Sigma = 0.5$, $\mu_\Pi = -0.5$. Top: quantum calculations. Bottom: semiclassical calculations. See text for discussion.

solid lines in Fig. 3 is of course not specific to molecules and will be described elsewhere [28]; although it is based on the same physical idea, our derivation proceeds differently to that given in [27], and yields different results. We have included the contribution of the on-node perpendicular orbit in the semiclassical calculations shown on Fig. 2.

2. Multiple core scattering

We have plotted in Fig. 4 the quantum and semiclassical recurrence spectra for the choice of quantum-defects $\mu_\Sigma = 0.5$, $\mu_\Pi = -0.5$. Although such a combination is quite unphysical for typical molecules, the examination of this case is instructive. The graphic reveals two striking aspects: first, the amplitude of the orbits associated with the core in state $N = 2$ are much stronger than the amplitudes of the orbits associated with the ground state $N = 0$ of the core; second, there is a strong discrepancy in the amplitude of the $N = 2$ orbits, which increases with increasing scaled action.

In the cases presented in Figs. 2(c) and 2(d), both elastic and inelastic scattering was allowed, but the quantum transition factor for orbits with the core in $N = 2$ states was stronger for *inelastic* scattering, and elastic scattering for $N = 2$ orbits (including $N = 2$, $m = 0$ to $N = 2$, $m = \pm 1$ scattering) was weak [by quantum transition factor, we mean the quantum scattering related part of Eq. (31), $\Sigma_{\alpha,\alpha'} \langle j' | \alpha' \rangle \langle \alpha | j \rangle C_\alpha C_{\alpha'} e^{i\pi(\mu_\alpha + \mu_{\alpha'})} T_{jj'}$, which indeed factors the individual contributions of the classical orbits]. But when $\mu_\Sigma = 0.5$, $\mu_\Pi = -0.5$, this quantum factor vanishes for $E_j \neq E_{j'}$, thereby totally suppressing *inelastic* scattering. Moreover, *elastic* scattering between $N = 2$, $m = 0$, ± 1 orbits is enhanced, being about 60 times stronger than for the combination of quantum defects giving rise to Figs. 2(c) and 2(d). Hence, we have a quasiatomic situation for the orbits associated with the core in states $N = 2$, with strong elastic quantum scattering and strong classical amplitudes, the latter characteristic of the quasiregular regime which prevails at $\epsilon = -0.8$.

We may thus expect multiple core scattering to have an important effect. This is seen in Fig. 5, where we have plotted different recurrence spectra of the $N = 2$ orbits at $\epsilon =$
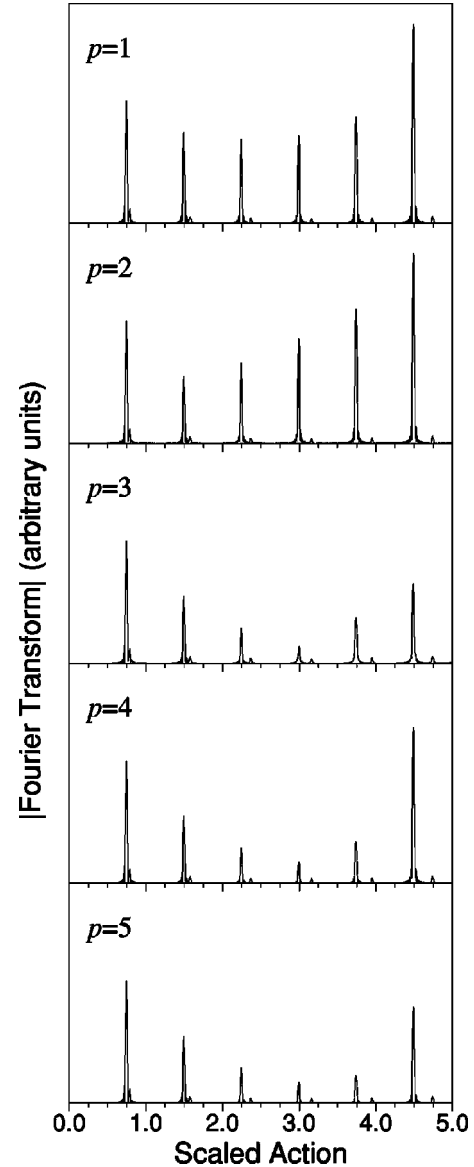

FIG. 5. Semiclassical calculations with allowance for multiple core scattering at $\epsilon = -0.8$, corresponding to the orbits associated with the core in state $N = 2$ shown in Fig. 4. Each successive panel adds an additional encounter with the core, and thus an additional orbit which interferes constructively or destructively. The number of core scatters is indicated by $p - 1$: $p = 1$ shows the hydrogenic recurrence spectrum, with the primitive orbits a,b, and their repetitions. $p = 2$ shows the situation after one core-scattering process, so for example, the peak at $\tilde{S} = 1.5$ results from the interference of the second repetition of a with the core-scattered orbit a+a. Convergence (for actions $\tilde{S} \leq 5$) is seen to be achieved after including five core scatters. Agreement with the quantum results (Fig. 4, top) is then obtained.

-0.8, each panel corresponding to an increase in the number of core scatterings. It is seen that convergence is achieved after five iterations, after which the semiclassical recurrence spectrum agrees with the quantum results. In short, although multiple core scattering is a higher-order effect (since each core-scattering process is suppressed by a factor $\hbar^{1/2}$ [$\hbar$ for the parallel orbit]), it must be taken into account when the

amplitudes are strong (which happens here with the $N=2$ orbits when elastic scattering dominates), or for higher actions of the recurrence spectra.

VI. DISCUSSION AND CONCLUSION

The theoretical developments presented in Sec. III called for the usual approximations involved in atomic closed-orbit theory, which has been interpreted and compared successfully to experimental spectra in both the fixed magnetic field and constant scaled-energy domains. However, an approximation made in Sec. III F, when we applied the ideas of scaled-energy spectroscopy to the molecule, is questionable. Indeed, to achieve the scaling we were led to artificially modify the rotational molecular constant because a molecular system does not scale exactly. From a theoretical point of view, the role of this approximation is to ease the extraction of the underlying classical dynamics. However, in an experimental situation, the magnetic field and the excitation frequency of the laser would be simultaneously adjusted so as to keep the scaled energy of the most excited electron (i.e., that associated with the molecular core in its ground state, in this case $N=0$) constant. When, say, the field intensity γ is increased while keeping $\epsilon_{N=0}$ constant, the electron associated with the excited core will encompass different dynamical regimes [and $\epsilon_{N=2}$ will vary according to Eq. (32)]. In general, $\epsilon_{N=2}$ will be contained within the quasiregular regime, which brings in simple dynamics since there are only two short-action closed orbits but the actions of those orbits do change, since the periods get shorter as $\epsilon \rightarrow -\infty$. Therefore, the physical mechanism that we described above, in which the spectral modulations are explained in terms of inelastic and elastic core scattering still holds (this mechanism is independent of the scaling properties of the system). But we do not expect a standard Fourier transform to give recurrence spectra as clean as those presented in Fig. 2, and other numerical methods (e.g., a γ-dependent Fourier transform) will need to be employed if the classical dynamics associated with the excited core states is to be extracted.

Further refinements can be included in the semiclassical theory. On the one hand, methods to correct the breakdown of the semiclassical approximation (divergences at bifurcations, "ghost" orbits) are well known, and these are not specific to the molecular extension—in fact, they only concern the hydrogenic classical dynamics, although in a molecular spectrum each mismatch arising from such a breakdown would be propagated through core scattering. On the other hand, the inclusion of further molecular perturbations, such as the provision for vibrational and electronic interactions can be included in the semiclassical theory. This is naturally included within the MQDT formalism by extending the frame transformation from a rotational to a rovibrational one, and replacing the short-range quantum defects μ_Σ, μ_Π by a nondiagonal matrix depending on the internuclear distance [15]. In this situation, a great number of Rydberg series interact, each built on a different rotational and vibrational state of the core. The spectral modulations will then essentially result from inelastic scattering between the outer electron and the molecular core.

In conclusion, we have presented the theoretical framework for a closed-orbit treatment of molecules in fields. The main extension was seen to be the combination of multichannel quantum scattering with hydrogenic closed orbits. We have also compared semiclassical and large R-matrix quantum calculations for a model molecule in a static magnetic field. The molecular core plays the role of an effective two-level scatterer: the ground state of the core was associated with classical trajectories of the electron in the chaotic regime, whereas the excited state of the core was associated with trajectories in the quasiregular regime. Hence, the core is intrinsically a quantum object, on which the semiclassical waves diffract, either elastically or inelastically. The agreement between semiclassical and quantum results were seen to be good, and the aspect of the recurrence spectra crucially depended on the value of the quantum defects.

APPENDIX A: HAMILTONIANS AND SCALED VARIABLES

In this appendix, we give the Hamiltonians for the hydrogen atom in a magnetic field and show how it can be scaled to remove the separate dependence on electron energy and field strength. Classically, the dynamics of a highly excited hydrogen atom (in a state with $m=0$) in the presence of an external static magnetic field aligned along the z axis is described by a single-particle, nonrelativistic Hamiltonian. Expressed in atomic units and cylindrical coordinates (ρ, ϕ, z), this is

$$H = \frac{1}{2}(p_\rho^2 + p_z^2) - \frac{1}{(\rho^2+z^2)^{1/2}} + \frac{1}{8}\gamma^2\rho^2, \quad (A1)$$

where γ is the magnetic field strength.

The classical motion of Hamiltonian (A1) exhibits an important scaling property. If we transform variables according to

$$\tilde{r} = \gamma^{2/3}r, \quad \tilde{p} = \gamma^{-1/3}p, \quad \tilde{t} = \gamma t, \quad (A2)$$

we obtain the *scaled* Hamiltonian

$$\tilde{H} = \frac{1}{2}(\tilde{p}_\rho^2 + \tilde{p}_z^2) - \frac{1}{(\tilde{\rho}^2 + \tilde{z}^2)^{1/2}} + \frac{1}{8}\tilde{\rho}^2 = \epsilon, \quad (A3)$$

which is simply the original Hamiltonian of Eq. (A1) multiplied by $\gamma^{-2/3}$. In terms of the scaled variables, the classical dynamics no longer have a separate dependence on the energy of the electron E, and field strength but is governed by the single parameter, the *scaled energy* $\epsilon = E\gamma^{-2/3}$.

In order to solve numerically the equations of motion generated by Hamiltonian (A3), it is convenient to make a regu-

larizing transformation that removes the Coulomb singularity. For the case considered here, where $m=0$, this can be achieved by transforming to semiparabolic coordinates, (u,v), where

$$u^2 = \tilde{r} + \tilde{z}, \quad v^2 = \tilde{r} - \tilde{z}, \quad \text{with} \quad \tilde{r} = (\tilde{\rho}^2 + \tilde{z}^2)^{1/2}, \quad \text{(A4)}$$

and with conjugate momenta, $p_u = du/d\tau$, $p_v = dv/d\tau$, defined with respect to a rescaled time, τ, given by

$$\frac{d\tau}{dt} = \frac{1}{2\tilde{r}(t)} = \frac{1}{(u^2 + v^2)}. \quad \text{(A5)}$$

On transforming to semiparabolic coordinates our final Hamiltonian becomes

$$\mathcal{H} = \frac{1}{2}(p_u^2 + p_v^2) - \epsilon(u^2 + v^2) + \frac{1}{8}u^2 v^2 (u^2 + v^2) - 2 \equiv 0. \quad \text{(A6)}$$

Strictly, the Hamiltonian of Eq. (A6) is only valid for $m=0$. However, for $m \neq 0$, the potential-energy surface differs from that for $m=0$ only close to the z axis where a centrifugal barrier now exists. Away from this small region near the z axis, the classical dynamics for small $m \neq 0$ differs only slightly from that at $m=0$ and hence we find it convenient to use the $m=0$ values in our calculations. The phase change arising in the semiclassical wave function because the $m \neq 0$ orbits no longer cross the z axis but are instead reflected at the centrifugal barrier is readily incorporated into the Maslov index.

The scaling transformation, Eq. (A2), has an important consequence for the quantum system. Solving the Schrödinger equation corresponding to Hamiltonian (A3) at fixed scaled energy leads to a set of eigenvalues $\{\gamma_i^{2/3}\}$ corresponding to a set of energies $\{E_i = \epsilon \gamma_i^{2/3}\}$. Thus, the field strength is not entirely eliminated from the quantum problem. Now, each E_i corresponds to a different value of an effective Planck's constant, the value of which is obtained by considering the position-momentum uncertainty relation in the *scaled* variables, e.g., $[\tilde{p}_\rho, \tilde{\rho}] = \hbar_{\text{eff}} = \gamma^{1/3}$. However, all of the eigenvalues now correspond to a *single* classical regime and the semiclassical limit, $\hbar_{\text{eff}} \rightarrow 0$, can be studied by decreasing the field strength while keeping ϵ constant.

We also define the classical *scaled action* of the kth closed orbit, which enters into the phase of the semiclassical wave function, as

$$\tilde{S}_k = \frac{1}{2\pi} \oint \tilde{p} \cdot d\tilde{q} = \frac{\hbar_{\text{eff}}}{2\pi} S_k, \quad \text{(A7)}$$

where we introduced the arbitrary 2π factor in keeping with the usual convention.

APPENDIX B: BASICS OF MQDT

Multichannel quantum-defect theory [14,15] partitions the system into the outer electron (of radial coordinate r and orbital momentum l) and the residual ionic core. A standing-

wave function then takes the form

$$\psi^S(r) = \sum_\alpha |\alpha\rangle \sum_{\alpha'} c_{\alpha'} [\delta_{\alpha\alpha'} f_{l_\alpha}(r) - \tan(\pi\mu_{\alpha\alpha'}) g_{l_\alpha}(r)], \quad \text{(B1)}$$

where f_{l_α} (g_{l_α}) is a standing-wave Coulomb function regular (irregular) at the origin and $|\alpha\rangle$ is a compound notation accounting for the core state as well as the orbital part of the outer electron with the relevant angular momenta couplings; α is thus a set of "good" quantum numbers when the outer electron is coupled to the core, and $\tan \pi\mu_{\alpha\alpha'}$ are the elements of the coupled-frame reaction matrix K (in the present case, K is diagonal with elements $\tan \pi\mu_\alpha$); the phase shifts μ induced by the short-range interaction are known as "quantum defects." The c_α are expansion coefficients. However when the electron roams far from the core, an expansion in the uncoupled basis j is appropriate,

$$\psi^S(r) = \sum_j |j\rangle \sum_{j'} c_{j'} [\delta_{jj'} f_{l_j}(r) - K_{jj'} g_{l_j}(r)]. \quad \text{(B2)}$$

The two coupling schemes are related by a unitary frame transformation with elements $\langle j | \alpha \rangle$.

Equations (B1) and (B2) may also be obtained as a particular case of the Lippmann-Schwinger equations [16]. It then follows that the coupled solution with outgoing-wave boundary conditions is obtained as

$$\psi(r) = \sum_\alpha |\alpha\rangle c_\alpha [f_{l_\alpha}(r) + (2i)^{-1}(e^{2i\pi\mu_\alpha} - 1) g_{l_\alpha}^+(r)], \quad \text{(B3)}$$

where

$$g_{l_\alpha}^\pm = (g_{l_\alpha} \pm i f_{l_\alpha}) \quad \text{(B4)}$$

are outgoing and incoming Coulomb waves and we have assumed a diagonal scattering matrix. In the uncoupled basis, we have

$$\psi(r) = \sum_j |j\rangle \sum_{j'} c_{j'} [\delta_{jj'} f_{l_j}(r) + T_{jj'} g_{l_j}^+(r)], \quad \text{(B5)}$$

where the T matrix is obtained from the quantum defects by applying the frame transformation,

$$T_{jj'} = \sum_\alpha \langle j | \alpha \rangle \frac{e^{2i\pi\mu_\alpha} - 1}{2i} \langle \alpha | j' \rangle. \quad \text{(B6)}$$

The expansion coefficients $c_{j'}$ are related to the expansion coefficients in the coupled basis c_α by

$$c_\alpha = \sum_j \langle \alpha | j \rangle c_j; \quad \text{(B7)}$$

in the field-free case, the expansion coefficients are obtained by using the boundary conditions at infinity; in the presence of an external field, boundary conditions in a region where the external fields are weak will be used.
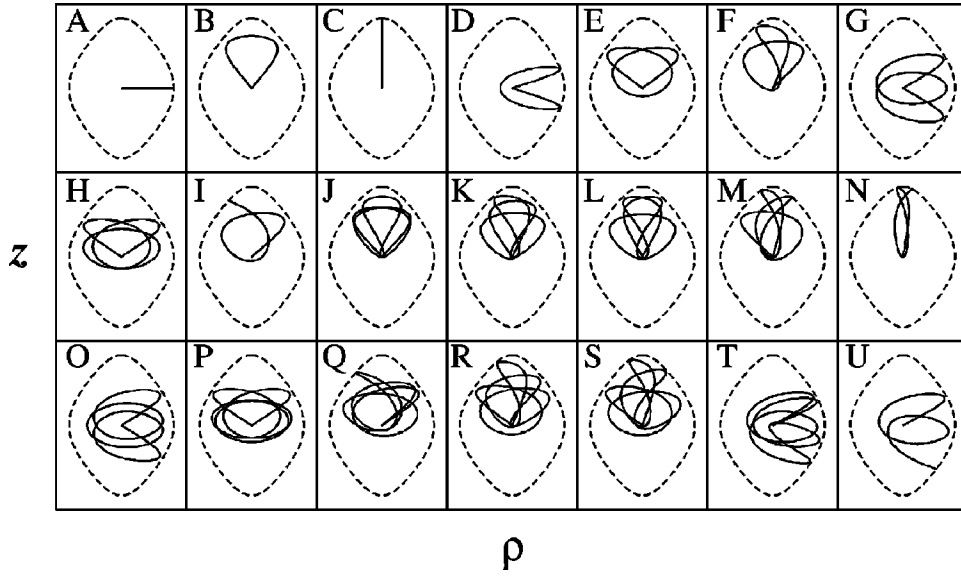
FIG. 6. Shapes of the classical closed orbits of the hydrogen atom in a magnetic field at a scaled energy of $\epsilon = -0.3$. The trajectories are plotted in the ρz plane and the dashed line denotes the energy surface. Only those orbits that contribute to the semiclassical recurrence spectra for scaled action $\tilde{S} \leq 5$ are shown. The labels A–U correspond to the key used to identify the orbits in Table I.

APPENDIX C: GREEN'S FUNCTION IN THE INNER ZONE

The molecular outgoing Green's function G in the inner zone is obtained by projecting the resolvent equation $G = G_0 + G_0 T G_0$, where G_0 is the Coulomb (long-range) molecular Green's function. G_0 can be shown to take the form [16]

$$G_0(r,r') = \sum_j |j\rangle\langle j| f_{l_j}(r) g^+_{l_j}(r') [2W^{-1}], \qquad (C1)$$

where $W = -(8\pi)^{-1}$ is the Wronskian of f and g^+ and we assume $r < r'$. Thus,

$$G(r,r') = -16\pi \sum_j |j\rangle g^+_{l_j}(r') \left\{ \sum_{j'} [\delta_{jj'} f_{l_{j'}}(r) \right.$$

$$\left. + T_{jj'} g^+_{l_{j'}}(r)] \langle j'| \right\}. \qquad (C2)$$

We also need to express the term between the curly braces in the coupled frame. Using Eq. (B6) along with the unitarity of the frame transformation yields

$$G(r,r') = -16\pi \sum_j |j\rangle g^+_{l_j}(r') \sum_\alpha e^{i\pi\mu_\alpha} \langle j|\alpha\rangle$$

$$\times [f_{l_\alpha}(r) \cos\pi\mu_\alpha + g_{l_\alpha}(r) \sin\pi\mu_\alpha] \langle\alpha|. \quad (C3)$$

APPENDIX D: CLASSICAL ORBITS

The properties of the classical orbits closed at the origin for an electron subjected to a Coulomb and a magnetic field are well known [6,8,25]. They are organized into "vibrators" V, along the z axis, "rotators" R, in the axial plane, and

exotics X. This terminology is given in Ref. [29]. Figure 6 shows all the closed orbits contributing to the semiclassical spectra for $\epsilon = -0.3$ up to a scaled action of $\tilde{S} = 5$. Table I gives the scaled action, Eq. (A7), and classical amplitude, Eqs. (D1) and (D2) with $\hbar_{\text{eff}} = 1$ for the first return to the nucleus of each of the closed orbits. The key A–U is used to identify each of the orbits with their shape as shown in Fig. 6 while the orbit label refers to the nomenclature of Ref. [29] where available. The peak label gives the numbers, corresponding to the labeled peaks in Figs. 2 and 4, at which the orbits and their repetitions contribute to the semiclassical spectrum. Note that, for orbits B, C, and D, we also give the amplitude at repeated returns to the nucleus together with the label of the corresponding peak to which they contribute. For completeness, we also include the data for the two classical orbits that contribute to the spectrum in the regular classical regime at $\epsilon = -0.8$.

The classical amplitude of the orbits A^j_k in the two-dimensional axial plane is determined from the evaluation of the 2×2 stability matrix in semiparabolic coordinates. We have [12]

$$\mathcal{A}^n_k = \hbar_{\text{eff}}^{1/2} |\sin\theta^n_{fk} \sin\theta^k_i|^{1/2} \left\{ \left| 2^{1/2} \cos\frac{\theta_{ik}}{2} \cos\frac{\theta^n_{fk}}{2} m_{12} \right|^{-1/2} \right\}$$

$$(\theta_{ik} \neq 0, \pi), \qquad (D1)$$

$$\mathcal{A}^n_k = \hbar_{\text{eff}} \{ |2^{1/2} m_{12}|^{-1} \} \quad (\theta_{ik} = 0, \pi), \qquad (D2)$$

where m_{12} is an element of the stability matrix for the nth return to the nucleus of the kth closed orbit. $\mathcal{A}^n_k$ is the result-

ing effective amplitude; the term between curly braces is $\tilde{r}_f^{-1/4} A_k^j$.

As is apparent from Eq. (D2), the treatment of the orbit parallel to the field ($\theta_{ik} = 0, \pi$) is special in many ways. The stationary phase derivation performed in Eqs. (18)–(20) is not valid in this case, resulting in a different $\hbar$ dependence, but there are other differences as well: each term between brackets in Eq. (31) needs to be multiplied by $h_{\text{eff}}^{1/2} 2^{-1/4} \pi^{-1/2} e^{-i\pi/2}$ when the orbit k or q is the parallel orbit. This change must also be incorporated in Eq. (36).

---

[1] H. Friedrich and D. Wintgen, Phys. Rep. **183**, 37 (1989).

[2] W. R. S. Garton and F. S. Tomkins, Astrophys. J. **158**, 839 (1969).

[3] A. R. Edmonds, J. Phys. (Paris), Colloq. **31**, C4-71 (1970).

[4] E. B. Bogomolnyi, Zh. Éksp. Teor. Fiz. **96**, 487 (1989) [Sov. Phys. JETP **69**, 2785 (1989)].

[5] M. L. Du and J. B. Delos, Phys. Rev. A **38**, 1896 (1988); **38**, 1913 (1988).

[6] J.-M. Mao, J. Shaw, and J. B. Delos, J. Stat. Phys. **68**, 51 (1992).

[7] J. Gao and J. B. Delos, Phys. Rev. A **46**, 1455 (1992).

[8] J. Main, G. Wiebusch, K. Welge, J. Shaw, and J. B. Delos, Phys. Rev. A **49**, 847 (1994).

[9] T. S. Monteiro and G. Wunner, Phys. Rev. Lett. **65**, 1100 (1990).

[10] D. Delande, K. T. Taylor, M. H. Halley, T. van der Veldt, W. Vassen, and W. Hogervorst, J. Phys. B **27**, 2771 (1994).

[11] M. Courtney, H. Jiao, N. Spellmeyer, and D. Kleppner, Phys. Rev. Lett. **73**, 1340 (1994); M. Courtney, N. Spellmeyer, H. Jiao, and D. Kleppner, Phys. Rev. A **51**, 3604 (1995).

[12] B. Hüpper, J. Main, and G. Wunner, Phys. Rev. Lett. **74**, 2650 (1995); Phys. Rev. A **53**, 744 (1996).

[13] P. A. Dando, T. S. Monteiro, D. Delande, and K. T. Taylor, Phys. Rev. Lett. **74**, 1099 (1995); Phys. Rev. A **54**, 127 (1996).

[14] M. J. Seaton, Rep. Prog. Phys. **46**, 169 (1983).

[15] C. H. Greene and Ch. Jungen, Adv. At. Mol. Phys. **21**, 51 (1985).

[16] A. Matzkin, Phys. Rev. A **59**, 2043 (1999).

[17] V. P. Maslov and M. V. Fedoriuk, *Semiclassical Approximation in Quantum Mechanics* (Reidel, Boston, 1981).

[18] B. E. Granger and C. H. Greene, Phys. Rev. A **62**, 012511 (2000).

[19] T. S. Monteiro and K. T. Taylor, J. Phys. B **22**, L191 (1989).

[20] M. Raoult, S. Guizard, and D. Gauyacq, J. Chem. Phys. **95**, 8853 (1991).

[21] X. H. He, K. T. Taylor, and T. S. Monteiro, J. Phys. B **28**, 2621 (1996).

[22] A. Matzkin and T. S. Monteiro, Phys. Rev. Lett. **87**, 143002 (2001).

[23] J. T. Hougen, *The Calculation of Rotational Energy Levels and Rotational Line Intensities in Diatomic Molecules*, Natl. Bur. Stand. (U.S.) Monograph No. 115 (U.S. GPO, Washington, DC, 1970).

[24] J. Main, C. Jung, and H. S. Taylor, J. Chem. Phys. **107**, 6577 (1997).

[25] J.-M. Mao and J. B. Delos, Phys. Rev. A **45**, 1746 (1992).

[26] J. Main and G. Wunner, Phys. Rev. A **55**, 1743 (1997).

[27] J. A. Shaw, J. B. Delos, M. Courtney, and D. Kleppner, Phys. Rev. A **52**, 3695 (1995).

[28] A. Matzkin, P. A. Dando, and T. S. Monteiro, ArXiv e-print physics 0207072.

[29] A. Holle, J. Main, G. Wiebusch, H. Rottke, and K. H. Welge, Phys. Rev. Lett. **61**, 161 (1988).